INTERNATIONAL JOURNAL FOR NUMERICAL METHODS IN FLUIDS
Int. J. Numer. Meth. Fluids **29**: 951–973 (1999)

FLUX-CORRECTED TRANSPORT TECHNIQUE FOR OPEN CHANNEL FLOW

SCOTT A. YOST* AND PRASAD M.S.V. RAO

161 CE/KTC Building, Department of Civil Engineering, University of Kentucky, Lexington, KY 40506-0281, USA

SUMMARY

In modeling flow in open channels, the traditional finite difference/finite volume schemes become inefficient and warrant special numerical treatment in the presence of shocks and discontinuities. The numerical oscillations that arise by making use of a second- and higher-order schemes require some additional smoothing mechanism. A characteristic feature of high-resolution schemes lies in smooth capturing of the shock fronts. This paper provides a general formulation for a flux-corrected transport algorithm to the one-dimensional open channel flow equations. The preliminary results presented show that the present algorithm is an efficient, conservative and robust tool that can be easily coded. To demonstrate the robustness of the present formulation, results are compared with other published numerical results, experimental data and analytical solutions when available. In particular, a comprehensive study on the effect of the source term, dry bed, variable width channel, steep sloping channel and flow with mixed flow conditions (as in a hydraulic jump) has been carried out to test the efficacy of the present algorithm. Copyright © 1999 John Wiley & Sons, Ltd.

KEY WORDS: flux correction; open channel; hydraulic jump; dry/wet bed; surge; finite difference; numerical modeling

1. INTRODUCTION

A major difficulty in the numerical approximation of non-linear hyperbolic conservative equations that describe the flow in open channels is the presence of discontinuities or shock fronts. Physically, the flow field discontinuities do not exhibit oscillations. On the other hand, many numerical solutions exhibit oscillations. Thus, these oscillations are purely of numerical origin and the extent of the oscillation is a feature of the numerical approach. Traditional explicit finite difference methods (i.e. Lax-Wendroff, MacCormack or any other higher-order schemes) that perform very well in smooth flow conditions, generate spurious oscillations (also referred to as 'wiggles', 'undershoots/overshoots') in the vicinity of a shock front. Suppressing these oscillations in the vicinity of the shock lead to the addition of numerical smoothing terms (i.e. artificial viscosity). One of the more popular smoothing mechanisms is the procedure suggested by Jameson *et al.* [1]. Furthermore, central finite difference (FD) schemes of second or greater accuracy produce dispersive errors in capturing the shock profile. Specifically, the FD schemes have a poor resolution in this shock capturing ability (i.e. the shock discontinuity often traverses several grid nodes). To overcome the above two limitations, standard methods based on central differencing have often been replaced by high-resolution shock capturing schemes.

* Correspondence to: 161 CE/KTC Building, Department of Civil Engineering, University of Kentucky, Lexington, KY 40506-0281, USA. Tel.: +1 606 2574816; fax: +1 606 2574404; e-mail: yostsa@engr.uky.edu

CCC 0271–2091/99/080951–23$17.50

Received 16 September 1997
Revised 9 March 1998

To enjoy the advantages of higher-order schemes coupled with an oscillatory free solution, over the past decade focus has shifted toward developing and solving the flow equations with high-resolution schemes. These include the total variation diminishing (TVD) schemes of Harten [2], flux-corrected transport (FCT) methods of Boris and Book [3,4] and Zalesak [5], switches and cell-averaged piecewise fits utilized in the piecewise parabolic method (PPM) of Collela and Woodward [6] and the essentially non-oscillatory (ENO) schemes of Harten and Osher [7] and Shu and Osher [8].

Although all the above cited high-resolution schemes perform equally well for one-dimensional flows, the experience of the authors [9] indicate that the explicit FCT algorithm of Boris and Book [3] and Book and others [4] is more robust for open channel flows. The FCT algorithms can be easily coded and their extension to higher-dimensional flows is straight forward [5]. Higher-order accurate standard central difference schemes need an explicit inclusion of an artificial viscous term, not only to obtain a monotonous (i.e. oscillatory free) solution, but in many cases to keep the code functioning. In contrast, the solution obtained by using a FCT technique is monotonous.

Application of a FCT technique involves three basic stages: transportation (advection), diffusion and anti-diffusion [3]. While the latter two are salient aspects of any FCT technique, the nature in which the solution traverses from one node to another is a function of the numerical scheme. As the solution at the new time level is not known *a priori*, the regions where the solution needs to be diffused (i.e. the regions where dispersive errors are evident) are not known. Hence, the FCT approach diffuses the solution through out the computational domain, and then anti-diffuses (the opposite of diffusion) the solution. Though the magnitude of the anti-diffusion is equivalent to diffusion in uniform flow conditions, its value varies in the vicinity of the shocks. The criteria that determine whether the diffused fluxes should be completely canceled out by anti-diffusion is built into the 'flux limiter'. It is this interaction between the diffusion and anti-diffusion that enables the FCT techniques to capture shocks smoothly. Furthermore, FCT methods are independent of the discretization and hence they are easily portable. Thus, coupling the FCT approach to standard finite difference schemes will vastly improve the quality of the solution.

The equations that describe the flow in open channels are hyperbolic and non-linear in nature. As analytical solutions exist only for simple flow cases, they have been solved numerically using many different numerical approaches. In dealing with the oscillations, historically the focus has been to use shock capturing algorithms versus using shock fitting methods. To the authors' knowledge, no systematic study has been reported on the advantages of using high-resolution schemes in open channel flow. Open channel flow applications, for which the standard numerical schemes have either failed or have proven to be ineffective, are the tests utilized in the present formulation. In addition, the problems selected in this investigation refer to a broad spectrum of open channel flows. This paper focuses on the application of a FCT algorithm to the one-dimensional open channel flow equations with emphasis on numerical results.

2. GOVERNING EQUATIONS

The basic governing equations that describe the one-dimensional open channel flows can be expressed in conservation form as [10]

$$[U]_t + [F]_x = [S], \tag{1}$$

where the elements of

$$[U]=\begin{bmatrix} A \\ Q \end{bmatrix}, \qquad [F]=\begin{bmatrix} Q \\ \dfrac{Q^2}{A}+\dfrac{gAh}{2} \end{bmatrix}, \quad \text{and} \quad [S]=\begin{bmatrix} 0 \\ gA(S_0-S_f) \end{bmatrix}$$

in which A is the flow depth, Q is the flow discharge, g is the gravity term, S_0 is the bottom slope of the channel and S_f is the frictional slope, which is computed from Manning's equation. For wide channels, it is given as [10]

$$S_f=\frac{u^2 m_n^2}{h^{4/3}}, \tag{2}$$

where u is the flow velocity, m_n is the roughness coefficient and h is the flow depth.

3. NUMERICAL PROCEDURE

The numerical implementation of the FCT technique for the governing equations is presented in this section. Though this work focuses on one-dimensional flows, it can be extended directly to higher-dimensional flows [5]. Starting from the initial time level where all the flow variables are known at all grid nodes, the following numerical procedure is followed [4]. First, the fluxes are transported to the unknown time levels by using any traditional higher-order numerical scheme. This work uses the two-step Lax-Wendroff technique. The unknown solution at the new time level, $n+1$ (see Figure 1), is obtained by first computing the flow variables at an intermediate time level $(n+1/2)$ as

$$U_{i+1/2}^{n+1/2}=\frac{1}{2}(U_i^n+U_{i+1}^n)-\left(\frac{\delta t}{2\,\delta x}\right)(F_{i+1}^n-F_i^n). \tag{3}$$

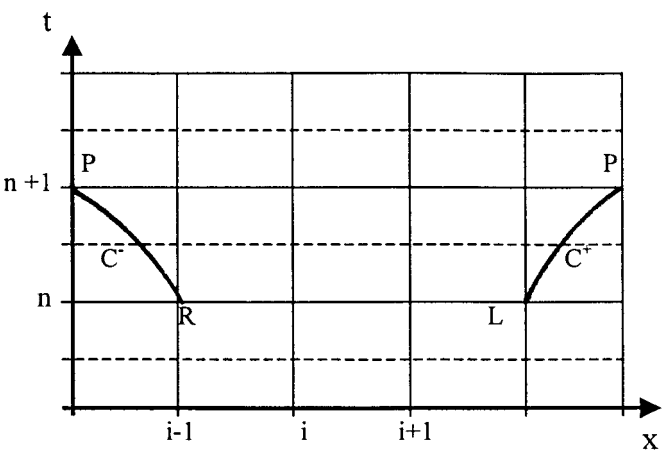

Figure 1. One-dimensional finite difference discretization along with the characteristic lines.

The solution is advanced the full time step by making use of Equation (3) to update the fluxes, or

$$U_i^{n+1} = U_i^n - \left(\frac{\delta t}{\delta x}\right)(F_{i+1/2}^{n+1/2} - F_{i-1/2}^{n+1/2}). \tag{4}$$

Next the diffusive flux from the first difference of U_i^n is computed by

$$D_{i+1/2}^n = \eta(U_{i+1}^n - U_i^n) \qquad D_{i-1/2}^n = \eta(U_i^n - U_{i-1}^n). \tag{5}$$

The anti-diffusive flux, A, from the first of U_i^{n+1} is computed using

$$A_{i+1/2}^{n+1} = \eta(U_{i+1}^{n+1} - U_i^{n+1}) \qquad A_{i-1/2}^{n+1} = \eta(U_i^{n+1} - U_{i-1}^{n+1}). \tag{6}$$

With this information, the values of Equation (4) are updated using the first difference of the diffused fluxes, Equation (5):

$$U_i^{n+1} = U_i^{n+1} + D_{i+1/2}^n - D_{i-1/2}^n. \tag{7}$$

The solution obtained by Equation (7) needs to be anti-diffused. Namely, the diffusion added in regions not requiring a diffused solution needs to be canceled. This is usually done by using a flux limiter, which is given as

$$L_{i+1/2}^{n+1} = S \max\{0, \min \lfloor S(U_i^{n+1} - U_{i-1}^{n+1}), S(U_{i+2}^{n+1} - U_{i+1}^{n+1}), |A_{i+1/2}^{n+1}| \rfloor \}, \tag{8}$$

where

$$S = \begin{cases} +1 & \text{if} \quad A_{i+1/2}^{n+1} \geq 0 \\ -1 & \text{if} \quad A_{i+1/2}^{n+1} < 0 \end{cases}.$$

Finally, the updated solution of Equation (7) is corrected for excess diffusion by using the first-order difference of the limited fluxes:

$$U_i^{n+1} = U_i^{n+1} - L_{i+1/2}^{n+1} + L_{i-1/2}^{n+1}. \tag{9}$$

The values of the flow variables at all the interior nodes are computed by using Equation (9). Appropriate boundary conditions are applied, thus completing the computation at the new time level. The coefficient η used in Equations (5) and (6) is known as the diffusivity coefficient. A note on the choice of the magnitude of η is timely. The primary purpose of a diffusion coefficient lies in smoothing the oscillations that arise in the numerical solution and its magnitude depends on the gradient of flow, grid spacing and time step. Its magnitude can be a either carefully selected input parameter [1,10] or calculated at the end of every time using the computed flow variables. In this work, the authors had calculated it using the equations suggested by Book *et al.* [4].

$$\eta = \varepsilon/(1 + 2\varepsilon)^2, \tag{10}$$

where $\varepsilon = \max(u_j \, \Delta t/\Delta x)$ with $1 \leq j \leq$ number of grid nodes. While Equation (10) indicates that η is a function of the advective velocity, the results obtained by relating it to the gravity wave speed as $\varepsilon = \max\{(u + \sqrt{gh})_j \, \Delta t/\Delta x\}$, did not change the results significantly.

4. STABILITY CONDITION

The CFL stability condition that governs the choice of time step in the numerical solution of Equation (1) can be written as [10]

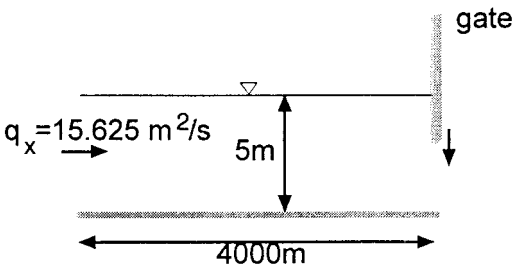

Figure 2. Definition sketch for sudden closure of gate.

$$\delta t = C_n \frac{\Delta x}{\max(|u| + \sqrt{gh})}, \tag{11}$$

where C_n is the Courant number (≤ 1) and Δx is the grid spacing. With selected grid spacing and known flow conditions, the time step is computed using Equation (11).

5. APPLICATIONS

With the highlights of the numerical scheme outlined, several computational tests have been performed to study the method's performance on a wide variety of one-dimensional open channel flows, with particular focus on its shock capturing ability. To illustrate the method, results are presented for shocks that are often formed by a sudden opening or closing of a gate, oscillating wave, dam break in horizontal and sloping channels with both wet and dry beds, and the formation of a hydraulic jump. The first three examples have been selected for benchmarking purposes since analytical solutions are available. These tests demonstrate the built in advantages of the present technique while illustrating the FCT's robustness in solving the 1D open channel flow equations (Equations (1) and (2)). Unless otherwise noted, all the cases studied utilize a Courant number of 0.8 in determining the time step, which is based on the CFL stability condition [10].

5.1. Simulation of surges

Surges in open channels frequently arise due to either a sudden opening or closing of a control gate. The hydraulic events that follow sudden gate movement are important aspects in the design of channels. Emphasis is placed on satisfactory prediction of both the arrival time of the wave front and its height. A comparison of the numerical results with the analytical solutions is presented to demonstrate the abilities of the FCT approach before analyzing more complicated flows.

5.1.1. Sudden closure of a gate. The hydraulic characteristics arising out of a sudden closure of the downstream gate is studied. The definition sketch of the test problem is shown in Figure 2. The test problem consists of a unit width horizontal rectangular channel 4000 m long with an initial depth and specific discharge of 5 m and 15.625 $m^2 s^{-1}$ respectively. To facilitate a comparison with the analytical solution, the channel is assumed to be frictionless (i.e. zero roughness coefficient). A surge was created at the downstream end by an instantaneous closure of the gate. The initial conditions of $h = 5$ m and $q_x = 15.625$ $m^2 s^{-1}$ were specified throughout the channel domain. Numerically, specifying a zero discharge at the downstream boundary creates the surge wave. Physically, this corresponds to the case of an instantaneous closure of

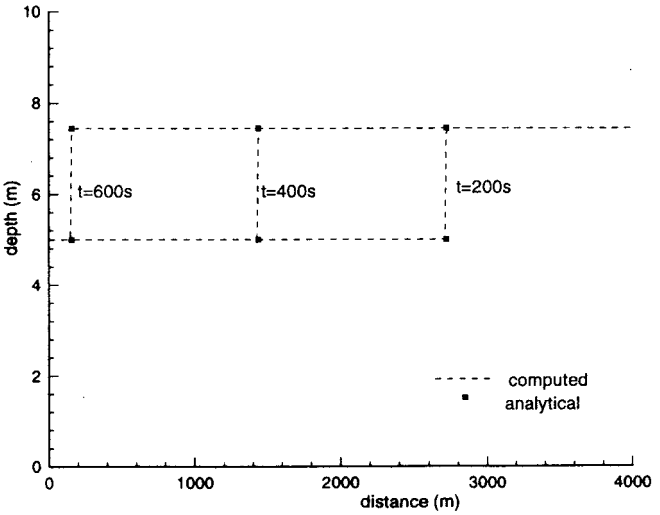

Figure 3. Transient profiles for a sudden closure of gate.

the gate. The other flow variable at the downstream boundary (i.e. flow depth) was calculated using the C^+ characteristic curve resulting from Equation (1), which is given as

$$q_P = q_L - \left\{ -\frac{q}{h} + \sqrt{gh} \right\}_L (h_P - h_L), \tag{12}$$

where the subscripts P and L are defined in Figure 1.

With a grid spacing $\Delta x = 4$ m, the surge generated by the gate closure was simulated until the wave reached the upstream boundary. Figure 3 compares the transient profiles with the analytical solution at three different time periods. The analytical solution for the above problem, derived by Abbott [11], is used as the benchmark. The plot indicates that the present FCT formulation can capture the shock front smoothly with high nodal resolution, an aspect absent in the standard finite difference formulations.

5.1.2. Sudden opening of a gate. A sudden opening of the gate is simulated by a sudden increase in the discharge at the upstream end of the channel containing a uniform water depth and no flow. The definition sketch of the problem is illustrated in Figure 4. The initial condition in the 4000 m long unit width frictionless channel is a uniform depth of 1 m with $q_x = 0$ m^2 s^{-1}. At the upstream boundary, a discharge of 10 m^2 s^{-1} is specified at time $t = 0^+$. At the downstream end, no boundary conditions are specified and the flow variables are kept

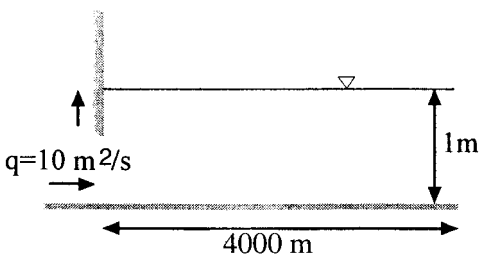

Figure 4. Definition sketch and boundary condition for a sudden opening of a gate.

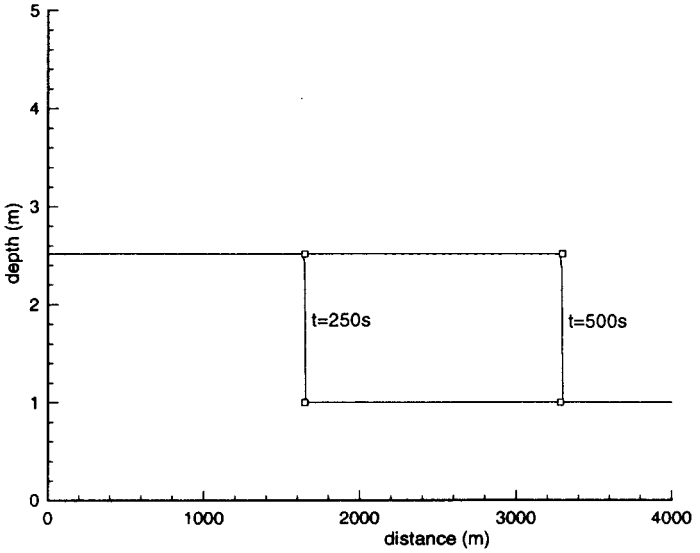

Figure 5. Transient profile for a sudden opening of a gate (---, computed; □, analytical solution).

at their initial values. The flow depth at the upstream boundary is computed from the C^- characteristic of Equation (1), which is given as

$$h_P = h_L - \frac{(q_P - q_L)}{\left(-\frac{q}{h} - \sqrt{gh}\right)_L}. \tag{13}$$

The gate opening was simulated with a grid spacing of $\Delta x = 4$ m. The evolution of shock front for two different times is plotted in Figure 5 along with the corresponding analytical solution. The predicted values of the celerity and the height of the wave front are in close agreement with the analytical solution with no oscillations evident near the shock front.

5.2. Modeling an oscillatory wave

This numerical test is concerned with the modeling of free oscillation in a horizontal frictionless rectangular channel that has an open boundary at the inlet and a closed boundary at the outlet. When it was first introduced into the field of computational hydraulics, Garcia and Kahawita [12] performed this test using the MacCormack scheme. This test is considered to be an extreme challenge for numerical models. Numerically, the free oscillation is accomplished by specifying an initial depth ($h_0 = 10$ m) and zero velocity ($q_x = 0$ m^2 s^{-1}) throughout the channel. Then a disturbance is created at the upstream boundary by suddenly increasing the depth, $h_t = 10.1$ m at $t = 0^+$, which is then held constant for all times. At the downstream end, a zero discharge is specified for all time, replicating a closed boundary. The other flow variables at the upstream and downstream boundary are computed from the C^- and C^+ characteristic curves respectively.

These specified boundary conditions generate an oscillatory wave whose wave height alternates between 10 and 10.2 m. The ability of the present formulation to capture this oscillatory wave nature is presented in Figure 6(a), which shows the time evolution of depth at the downstream boundary. No significant amounts of dissipation or oscillations are observed,

even for larger time periods, indicating the reliability of the present algorithm. A numerical scheme is considered satisfactory if it can reproduce the celerity and the time period accurately. The corresponding plot obtained by using the Lax-Wendroff technique without coupling it to the FCT approach is illustrated in Figure 6(b); oscillations near the shock front are evident. To further show the robustness of the algorithm, the transient discharge at the upstream boundary is plotted in Figure 7.

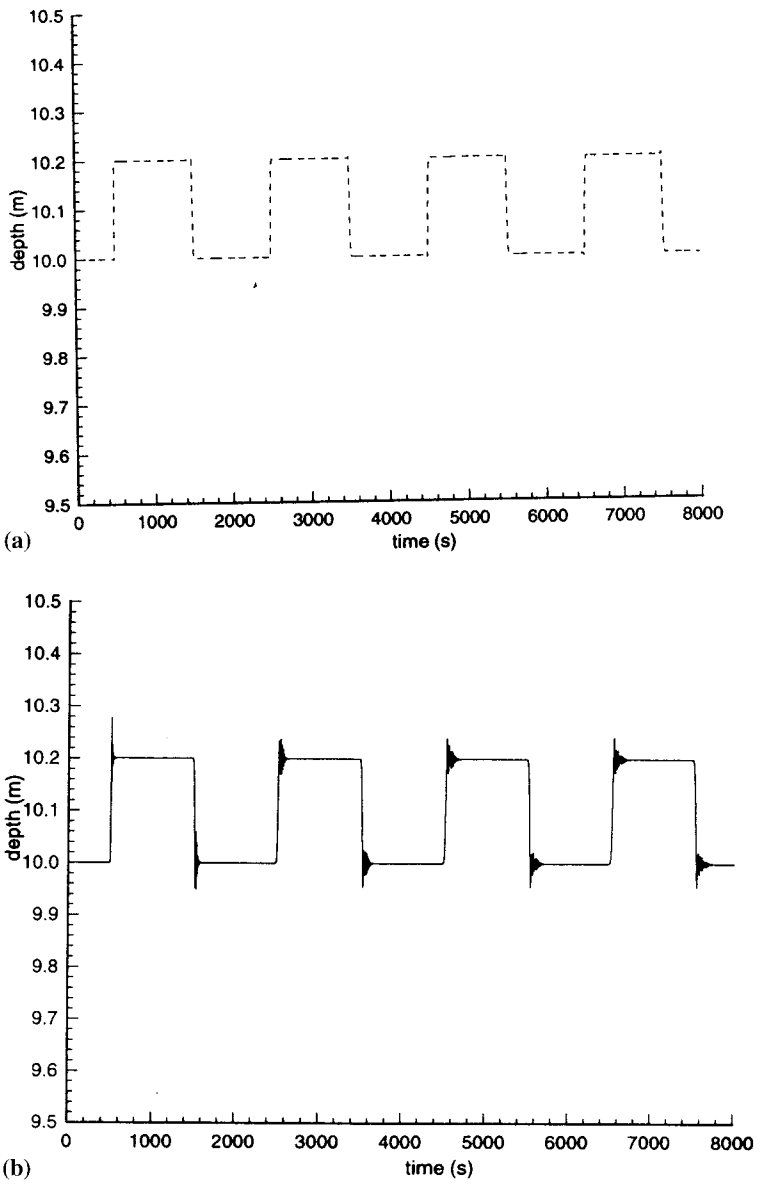

Figure 6. Transient profile of depth at downstream boundary: (a) with FCT and (b) without FCT.

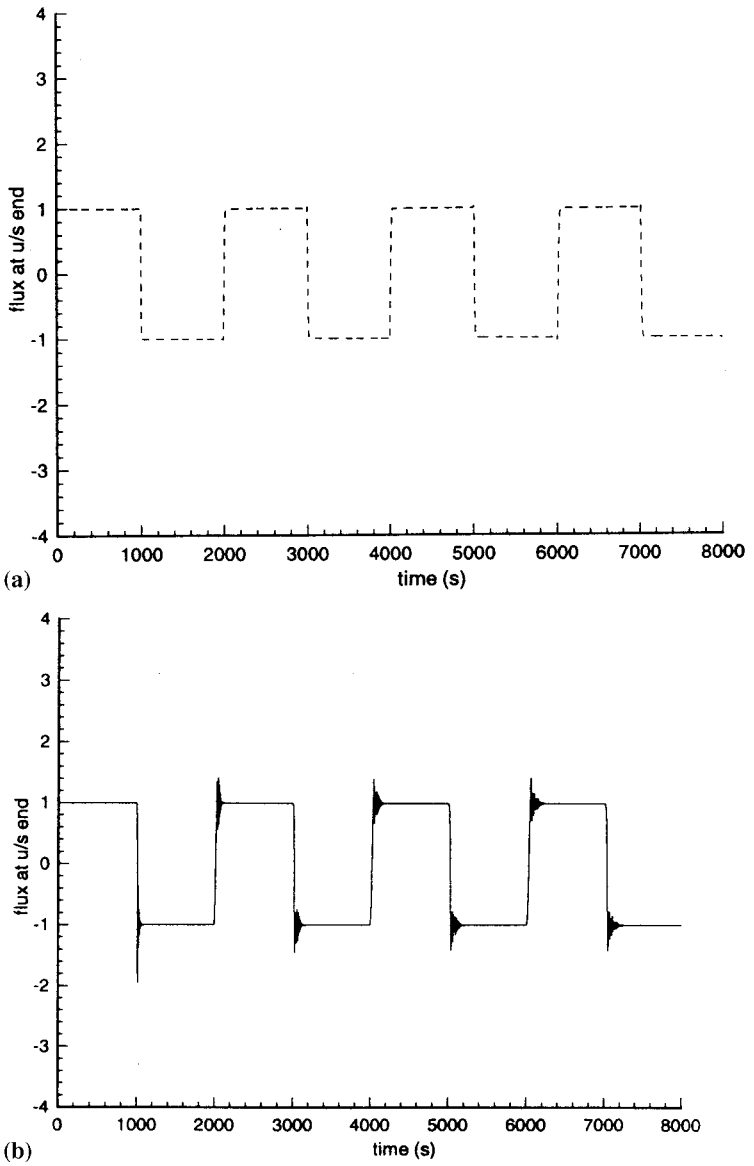

Figure 7. Transient discharge at upstream boundary: (a) with FCT and (b) without FCT.

5.3. Dam-break problem

The next test problem involves modeling of the progressive and regressive waves that are generated from the sudden failure of dam. As illustrated in Figure 8, a dam placed at the midsection of a horizontal rectangular channel of 4000 m is assumed to have given way instantly. The results for a depth ratio of 0.05 are reported herein. Figure 9 is a transient profile obtained at $t \cong 100$ s using a grid spacing of 4 m. While this test was repeated with several varying depth ratios, since no oscillations were evident at the downstream front for any case, only this one representative result is presented. Illustrating the direct benefit of the FCT

formulation, Figure 9 also shows the corresponding result obtained by decoupling the FCT approach ($\eta = 0$). For a detailed analysis, Table I compares five salient variables with the analytical values at $t \cong 100$ s. No appreciable amount of error is evident.

5.4. Simulation of a hydraulic jump

The capacity of the present model to simulate mixed flow conditions is tested by simulating a hydraulic jump, which is a challenging problem because of its complex nature. The hydraulic jump is formed whenever flow conditions change from supercritical to subcritical flow. Given its wide importance in open channel hydraulics, a proper simulation involves a satisfactory prediction of the location and height of the jump.

5.4.1. Description of experimental set-up. Since the present numerical simulations were chosen so that a comparison could be made with the experimental data, some brief information about the simulated channel is included. Further details of the experimental set-up and the methodology used in conducting the experiments can be obtained from Gharangik and Chaudhry [13]. The geometry of the rectangular metal flume is $14 \times 0.46 \times 0.915$ m^3. By suitably controlling the depth at the downstream end, the jump was allowed to form in the first 3.05 m of the glassed flume. The Manning's roughness coefficient varied between 0.008 and 0.011, depending on the depth. For the range of experiments reported, the Froude numbers of the incoming flows varied from 2.3 to 7.0. The flow variables for these Froude numbers are summarized in Table II.

5.4.2. Initial and boundary conditions. Initially, the flow is assumed to be supercritical throughout the channel. Starting with the specified initial conditions at the upstream end (Table II), the flow parameters at the other nodes are obtained by integrating the gradually varied flow equation [10]. As the flow is supercritical at the upstream end, it can be shown using the method of characteristics that all the flow information at the upstream end should be specified as a boundary condition. Hence, the depth and discharge at upstream boundary are specified and held constant for the entire simulation, equal to the initial values. At the downstream end, a constant flow depth is specified and held constant for all time. The other flow variable (discharge) is computed from the C^+ (positive) characteristic of Equation (1).

Since the focus is the steady state solution, a false transient approach was used. In this approach, the steady state solution is obtained by using time as an iteration parameter. Starting from the initial conditions ($t = 0$), the solution progresses until it reaches steady state. With the boundary conditions mentioned, the numerical approach is used to compute the unknowns at all the interior grid nodes.

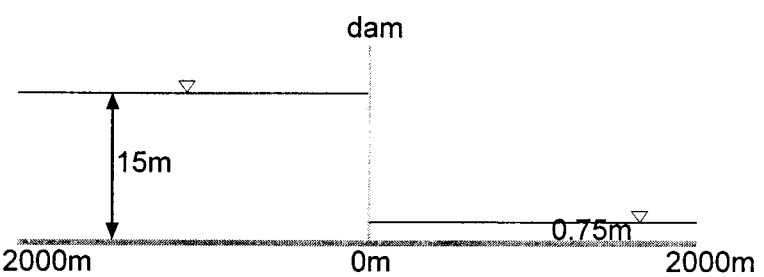

Figure 8. Definition sketch for sudden dam break case.

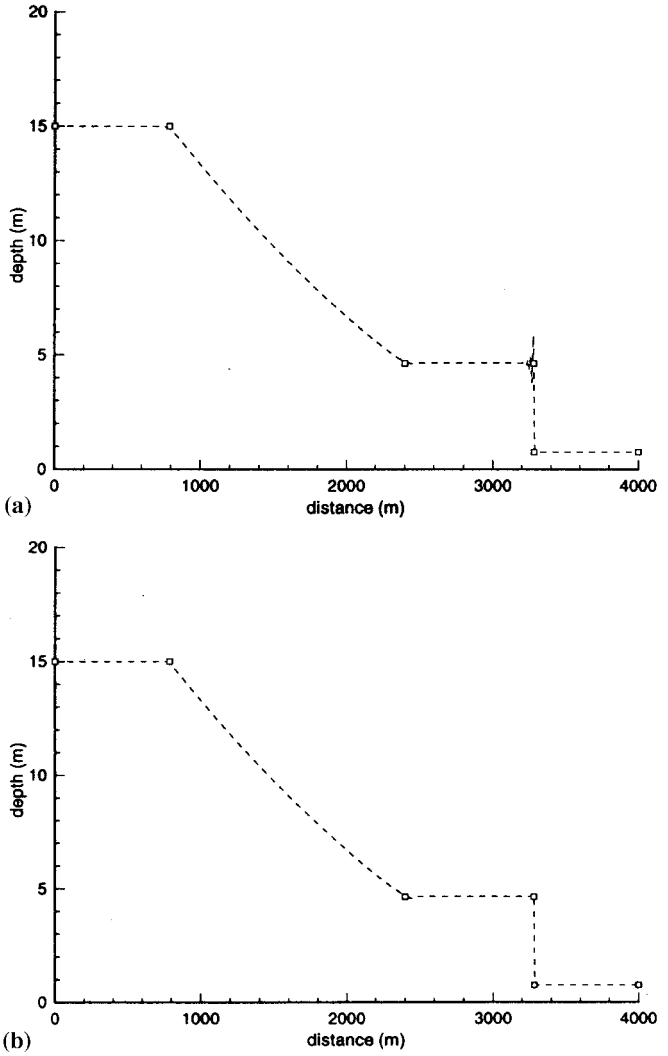

Figure 9. Transient profile for dam break at $t \cong 100$ s (□, analytical solution): (a) computed without FCT; (b) computed with FCT.

5.4.3. Results and discussion. Results for two Froude numbers cases ($F_r = 4.23$ and 6.00) are presented herein, although similar results were obtained for the other reported experimental cases as well. These results were obtained with a grid spacing of 0.28 m. However, before the results are discussed a brief mention on the validity of the governing equation (Equation (1)) is needed. The derivation of the governing equations, which are also known as the St. Venant equations, involves the assumption of hydrostatic pressure distribution. Though this assumption holds good for gradually varied flows, some modification may need to be done to the pressure term when the flow is rapidly varying, as in the case of a hydraulic jump. The contribution of an additional pressure term, which takes into account the non-hydrostatic pressure distribution has been numerically studied by Gharangik and Chaudhry [13] and Rahman and Chaudhry [14]. They conducted an order of magnitude analysis and concluded

Table I. Comparison between computed and analytical values

	Computed	Analytical	% Error
Depth at dam site (m)	6.71	6.67	0.6
Velocity at dam site ($m\,s^{-1}$)	8.03	8.08	0.6
Maximum height of shock front (m)	4.65	4.646	0.08
Speed of negative surge ($m\,s^{-1}$)	12.2	12.13	0.57
Shock speed ($m\,s^{-1}$)	10.72	10.75	0.28

that the extra pressure term contribution is very small near the flow transition and negligible in regions on either side of the shock front. With one of the side issues of the present work being to check the validity of Equation (1) without a modified pressure term, the results presented support the conclusion that no modification needs to be made to the pressure term.

The numerical modeling of the hydraulic jump was mainly focused on the application of finite difference schemes, because of their simplicity. Standard finite difference schemes have poor shock capturing ability in terms of their resolution, independent of the dispersive errors. Though the shock resolution can be improved by using a grid adaptation technique, it adds to the computational requirements and blurs the simplicity of the finite difference calculations. The grid spacing in an adaptation approach is non-uniform, with the underlying assumption that a large uniform grid spacing deteriorates the shock resolution and a small uniform grid spacing is often computationally uneconomical. Rahman and Chaudhry [14] first used this approach and were able to improve the shock resolution while using the MacCormack scheme (Jameson's procedure [1] was used to smooth the numerical solution). A grid adaptation [15] technique essentially tracks the location of the shock front, and decreases the grid spacing within the vicinity of the shock, thus keeping the width of the shock to a minimum number of grid nodes. In regions on either side of the shock where uniform flow exists, larger grid spacing is used.

The present FCT algorithm has a high-resolution shock capturing ability as an inherent feature. An extra grid equation does not need solving to achieve this, nor is there any additional mechanism required for smoothing numerical oscillations. Along with the experimental results, Figures 10 and 11 show the computed stationary hydraulic jump profiles for Froude numbers of 4.23 and 6.65 respectively. The FCT formulation captures the jump without oscillations at the shock front, independent of the Froude number. The shock front continues to form primarily between the two adjacent grid nodes, achieving the best possible resolution. Extensive tests on varying the grid spacing had no significant impact on the shock location. Again, to illustrate the direct benefits of the FCT formulation, an attempt was made to simulate the jump by without employing FCT (i.e. $\eta = 0$). The program failed to produce any output, indicating that some amount of artificial diffusion is necessary if FCT is not utilized. To verify the conservation of mass, the mass residual error was calculated. A small mass residual error of 0.1% ($F_r = 4.23$) and 0.098% ($F_r = 6.65$) was found, indicating that the

Table II. Test conditions for hydraulic jump [13]

Test number	Upstream depth (m)	Upstream velocity ($m\,s^{-1}$)	Downstream depth (m)	Froude number (F_r)
1	0.043	2.737	0.222	4.23
2	0.024	3.255	0.195	6.65

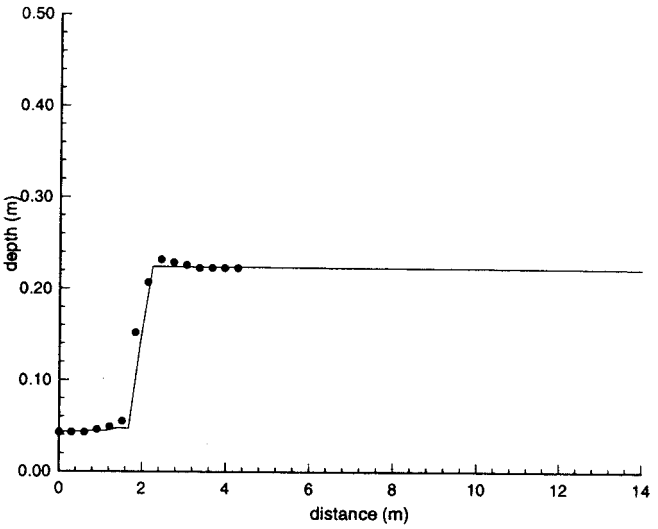

Figure 10. Stationary profile for $F_r = 4.23$ (---, computed; ●, experimental [13]).

present formulation (primarily diffusion and anti-diffusion) is in conservative form. Though the results are not included, similar results were also evident for simulated flows with other Froude numbers ($F_r = 2.3$, 5.74 and 7.00), indicating that the present formulation is a reliable and robust tool. The effect of Courant number on the location of shock front for $F_r = 6.65$ is shown in Figure 12. The numbers in brackets correspond to the values of the diffusivity constant, as computed using Equation (10), with η being the sum of advective velocity and gravity speed. No appreciable amount of phase errors is evident by including the gravity component. The effect of grid spacing for the same flow condition is shown in Figure 13. The plot indicates that the shock front is captured between the two adjacent nodes for the different grid spacing.

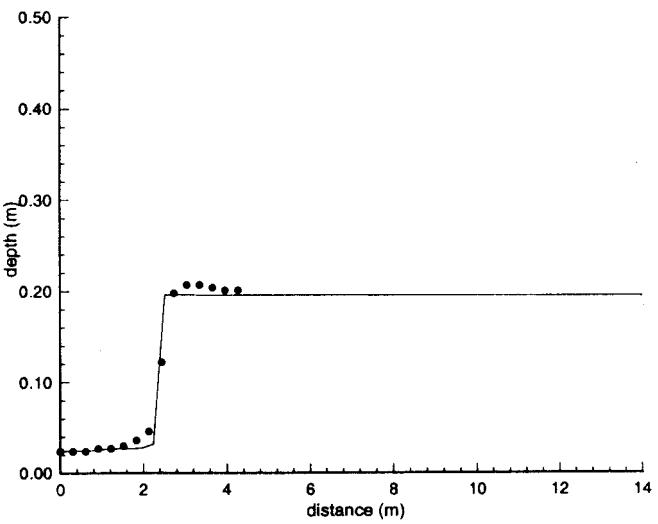

Figure 11. Stationary profile for $F_r = 6.65$ (---, computed; ●, experimental [13]).

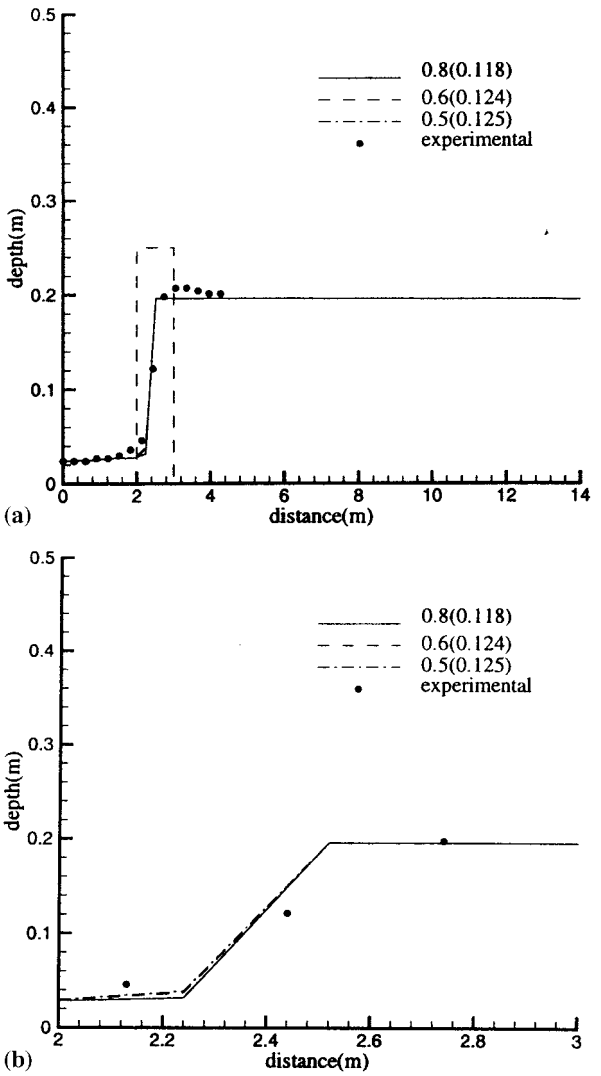

Figure 12. Effect of Courant number on shock front resolution ($F_r = 6.65$): (a) normal view, (b) zoom view.

While the FCT scheme works well when compared with the standard Lax-Wendroff method, Figure 14 compares the FCT shock profile with the profiles of two other high-resolution schemes, total variation diminishing [2] (TVD) and the essentially non-oscillatory [7] (ENO). As the formulation of TVD and ENO schemes are detailed in the references cited, no attempt has been made in this paper. As the magnitude of relative error (difference between the exact and computed solutions) is a reliable check of the efficacy of schemes, comparisons were made for three different flow cases, illustrated by Figures 3, 5 and 6(a), using the three different high-resolution techniques. The results of the relative error are summarized in Table III.

5.5. Flow on a variable width channel

The applicability of the present formulation has been tested on a dam break flow problem over a variable width channel. Though many numerical models have been applied in the recent past [12,16,17], the authors have no knowledge of any model being applied to variable width, sloping bed and a dry channel. Since analytical solutions are not available, the computational results are compared with the experimental data of Bellos *et al.* [l8]. In addition, several cases involving horizontal wet bed channels are compared with the numerical findings of Hicks *et al.* [17].

5.5.1. Description of experimental set-up. Bellos *et al.* [18] have conducted experiments on a rectangular flume with various flow and channel conditions. The flume, made of steel and glass, had a varying width along the flow axis as illustrated in Figure 15. A vertical plate acting as a dam was placed at the minimum width section ($x = 8.5$ m, $b = 0.6$ m). The observation points were distributed in both the upstream and downstream regions. The results obtained from Bellos *et al.* [18] include the flow depths measured as a function of time at five stations, $x = 0$, 4.5, 8.5, 13.5 and 18.5, which are used for comparisons. The flow, initially stationary throughout the length of the channel, was triggered by the sudden removal of the gate at the minimum width section (Station 3). This resulted in the generation of progressive and regressive waves, which traveled downstream and upstream respectively. No estimate of the errors in the observations or values of discharge at the measuring stations are reported in the experimental work.

Experiments were conducted for a wide range of bed slopes, dry and wet bed conditions as well as various upstream/downstream depth ratios. The range of bed slopes investigated is from 0 to 8%. The dry bed simulations had a zero initial flow depth, while the wet bed simulation had an initial flow depth of either 0.101 or 0.053 m. The upstream depths ranged from 0.15 to 0.30 m. However, no tests were conducted with a wet bed and a sloping channel.

The present model has been run for three test cases, representing the salient data of the above mentioned experimental results. The flow conditions and the channel conditions varied

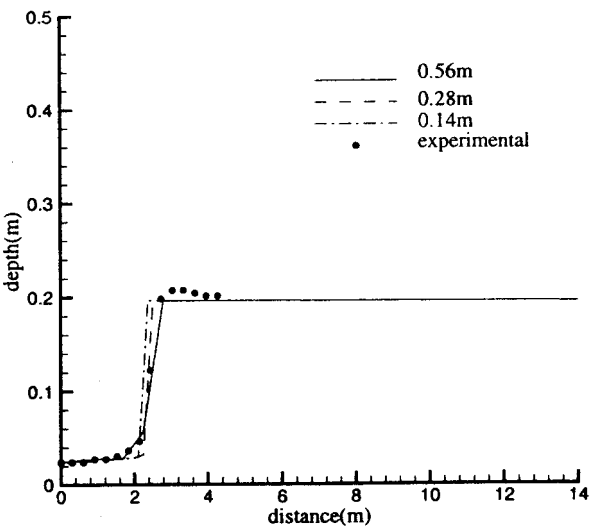

Figure 13. Effect of grid spacing on shock front resolution ($F_r = 6.65$).

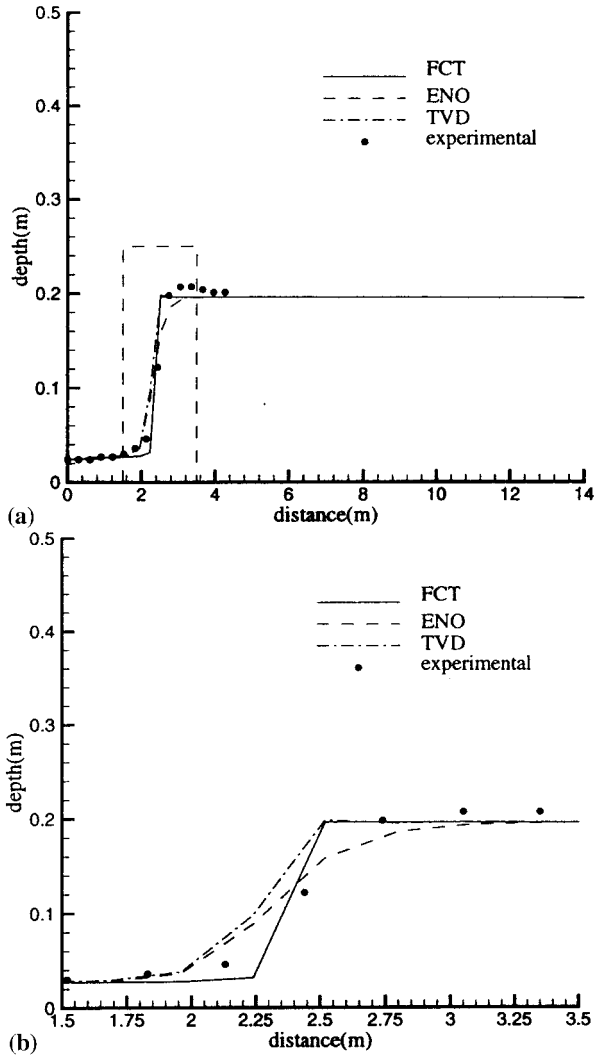

Figure 14. Profiles with different high-resolution schemes ($F_r = 6.65$): (a) normal view, (b) zoom view.

from set to set, summarized in Table IV. An initial zero discharge was specified throughout the computational domain. The boundary condition at the upstream boundary was a zero flow condition. The other flow variable, area, was made equal to its adjacent node value. As no specific information is available at the downstream end, the flow variables were interpolated from the interior nodes (non-reflective boundary). Since the downstream boundary was not

Table III. Comparison of error distribution (%)

	Figure 3 ($t = 400$ s)	Figure 5 ($t = 250$ s)	Figure 6(a)
TVD	6.7	4.7	1.6
ENO	5.1	3.4	1.7
FCT	3.9	1.6	1.6

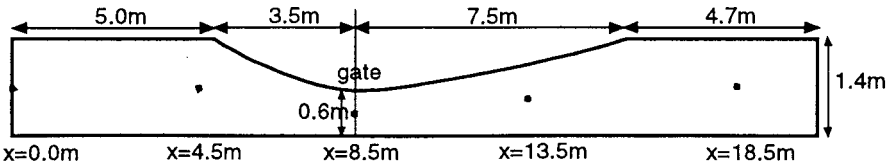

Figure 15. Plan view of constricted open channel with observations points (●).

detailed in the experimental results, numerical tests were conducted to investigate if the downstream boundary affected the solution at an observation point with the goal of minimizing any possible error that may be introduced due to an inappropriate boundary specification. However, increasing the length of the channel from 24 to 48 m for calculation purposes did not affect the flow depths at Station 5 ($x = 18.5$ m) for the first two cases. However, there are unknown boundary influences in Case III that are discussed below.

5.5.2. Results and discussion. In all three test cases a grid spacing of 0.25 m and a Manning's roughness coefficient of 0.012 were used in the simulation. The three cases correspond to horizontal flow on a dry bed (Case I), flow on sloping dry bed (Case II), and horizontal flow on wet bed (Case III). In each of the simulations, results are presented in comparison with the experimental results. In Case III, the results are also compared with Hicks *et al*. [17] since they have numerically studied the propagation of wave on a wet bed.

Case I: Modeling flow over a dry bed is computationally more challenging than flow over a wet bed. In order to minimize the computational difficulties, the standard procedure [19,20] is to assume a small finite amount of depth on the downstream side of the dam. However, Bellos and Sakkas [21] investigated this practice and have numerically shown that the celerity of the progressive wave, which is a function of the downstream depth, is adversely affected by the wet/dry initial condition. Hence, in this work, a zero flow depth has been specified at all the grid nodes on the downstream of the dam. A flow depth of 0.3 m on the upstream side, along with zero flow velocities, completes the initial conditions.

Figure 16 is a comparison of the computed transient depth profiles with the measured values at the five observation stations. In the simulations, it has been observed that the depth tends to take very small negative values. (The first negative depth was observed at $x = 9.5$ m. The depth was -1.18E-04, and the corresponding simulation time 0.22 s) Since the computation of friction factor (Equation (2)) and the time step (Equation (11)) depend on the flow depth, a negative value at any grid node results in stability problems. While this problem could be circumvented by assuming a finite amount of water depth in the downstream side, the results of Bellos [19] show that such a pseudo approach accelerates the propagation of the wave. To simulate the exact physical condition, the authors had assumed the downstream as a dry bed. As the negative flow depth is purely a numerical phenomenon that physically does not exist,

Table IV. Initial depth and channel bed conditions for variable width channel [18]

Case	Upstream depth (m)	Downstream depth (m)	Depth ratio	Bed slope (%)
1	0.3	0	—	0
2	0.25	0	—	6
3	0.2	0.101	2	0

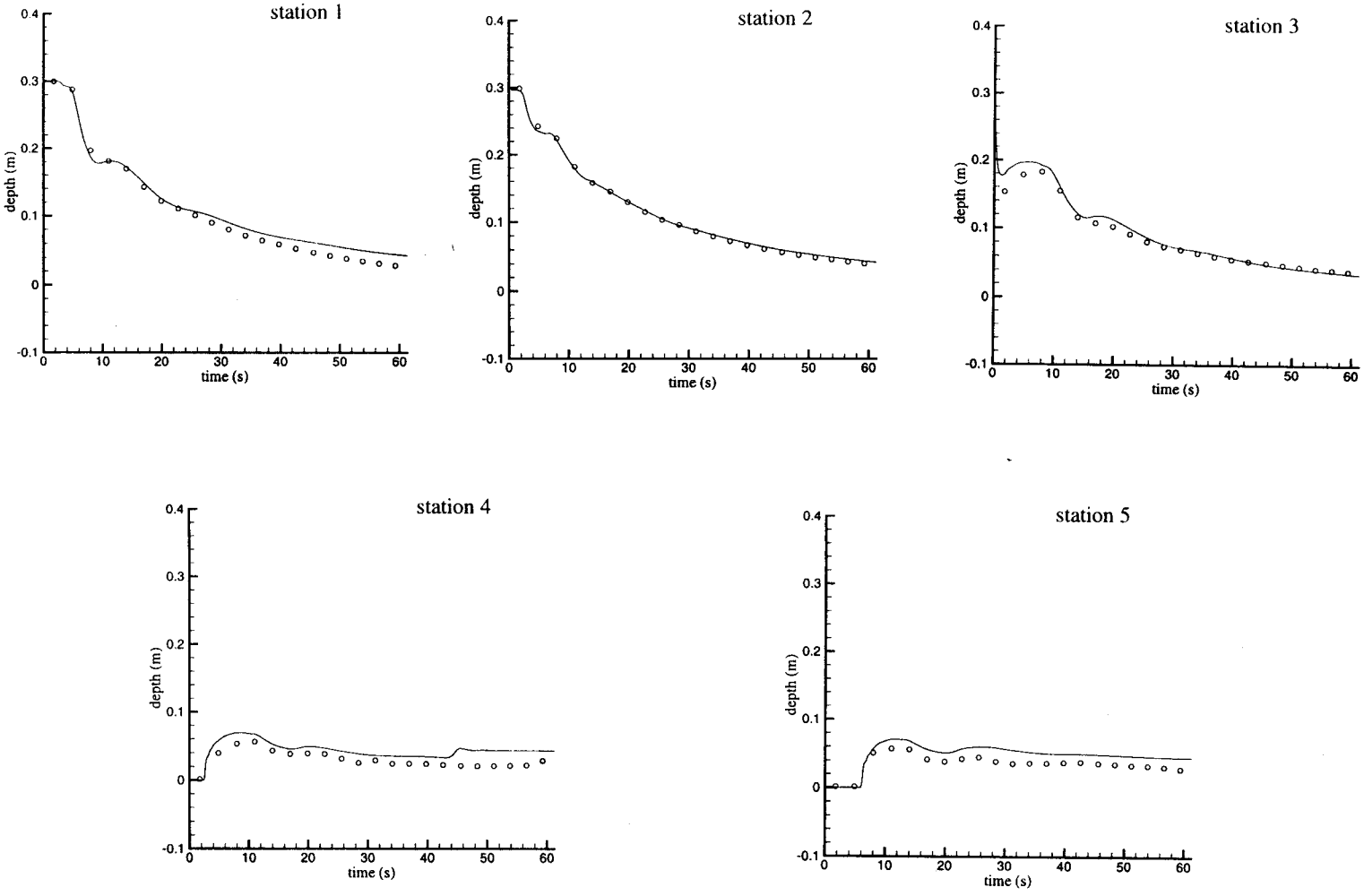

Figure 16. Comparison of numerical (—) and experimental [18] (○) results for a dry bed horizontal channel.

a small tolerance factor of 10^{-6} has been used to circumvent this problem. If the flow depth is less than 1×10^{-6} it is assigned a value of zero. Varying the tolerance factor and grid spacing did not affect the computed profiles. While the comparison of results at Stations 1, 2 and 3 is good, a small discrepancy is observed at Stations 4 and 5. A possible explanation for this is explained in the next section.

Case II: This case involves modeling flow over dry sloping bed. As the focus of this work is to test the present algorithm with the most numerically challenging problems, a steep slope of 6% was used. Along with a zero flow depth on the downstream side of the dam, an initial flow depth of 0.25 m was specified at the dam location ($x = 8.5$ m). The flow depths at all the other upstream grid nodes were computed to account for the bed slope.

Figure 17 is a comparison between the computed and measured depths at the five stations. As seen from the results, the present formulation reasonably matches the experimental results but overstates the depths at Stations 3 and 5 but understates the depths at Station 4. Part of the difference, both here and in Case I, can be explained in the context of the resistance coefficient. From gradually varied flow theory for open channels, resistance will increase the depth of flow. It is well-known that soil has a different resistance coefficient depending on if it is wet or dry. Thus, the leading edge of the dam break wave will experience a different resistance than that of flow over a dry bed. Since there is no way of knowing how the resistance varies, a constant value is assumed. By adjusting the resistance coefficient, one can effectively raise or lower the profile. However, the authors used the values published in the literature for all simulation.

Case III: This example studies the movement of a wave over a horizontal wet bed. As presented in Table IV, the initial flow depth is 0.2 m the upstream side of the dam and 0.101 m on the downstream side. As analytical solutions for a variable width channel are not available, the present computed depths are compared in Figure 18 with the numerical results of Hicks *et al.* [17] and to the experimental results [18]. The attempt made to run the code with a zero diffusivity coefficient (i.e. FCT turned off) did not yield any result, indicating that some smoothing mechanism for the oscillations is required. Hicks *et al.* [17] made use of a Petrov–Galerkin finite element method, and reported their results only for the first 18 s of flow. As can be seen from Figure 18, the results obtained in the present investigation are in close agreement with both the computational results and the experimental results at early times, but at later times the model underpredicts the depths. One can only speculate why this might be, but the authors believe the discrepancy is due to the downstream boundary condition, which was not reported in the original experimental work. In order to maintain an initial uniform depth of 0.1 m downstream of the dam, some type of weir was placed in the channel. For instance, if a weir 0.1 m high were used to maintain the initial water depth, after the wave reached the weir, a certain amount of water would flow over. However, there would also be a reflection from the weir boundary causing a wave to propagate upstream. This can be seen in the five different stations of Figure 18 as a jump in the water depth. The first occurring at about 16 s at Station 5, 20 s at Station 4, finally passing Station 1 at about 34 s. As this boundary reflection propagates upstream, the present model no longer maintains close agreement with the experimental observations. Since the exact boundary was not specified in the experimental work, no attempt was made to accommodate the unknown condition. Instead a uniform flux was assumed, albeit incorrectly.

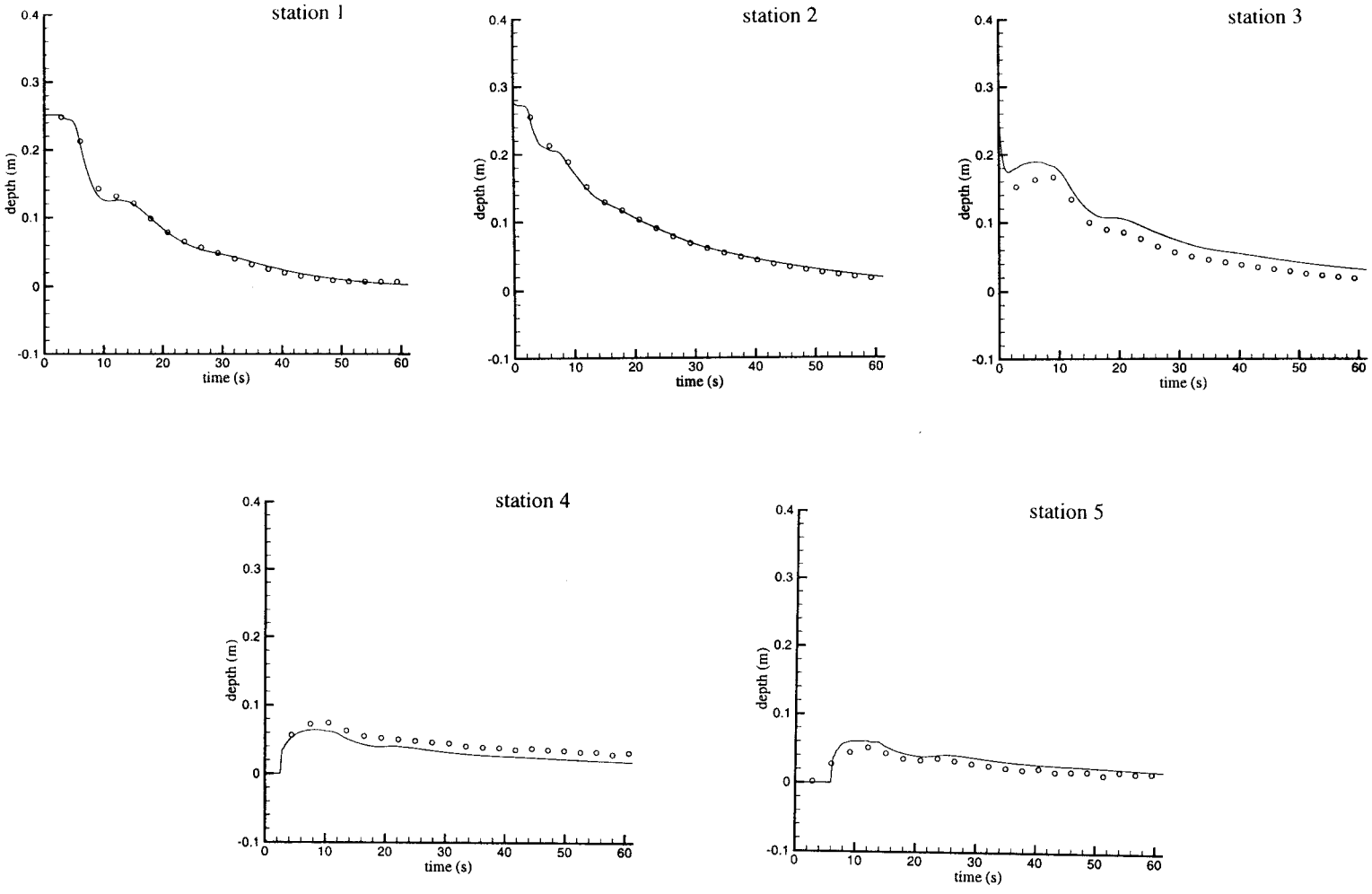

Figure 17. Comparison of numerical (—) and experimental [18] (○) results for a dry bed sloping channel.

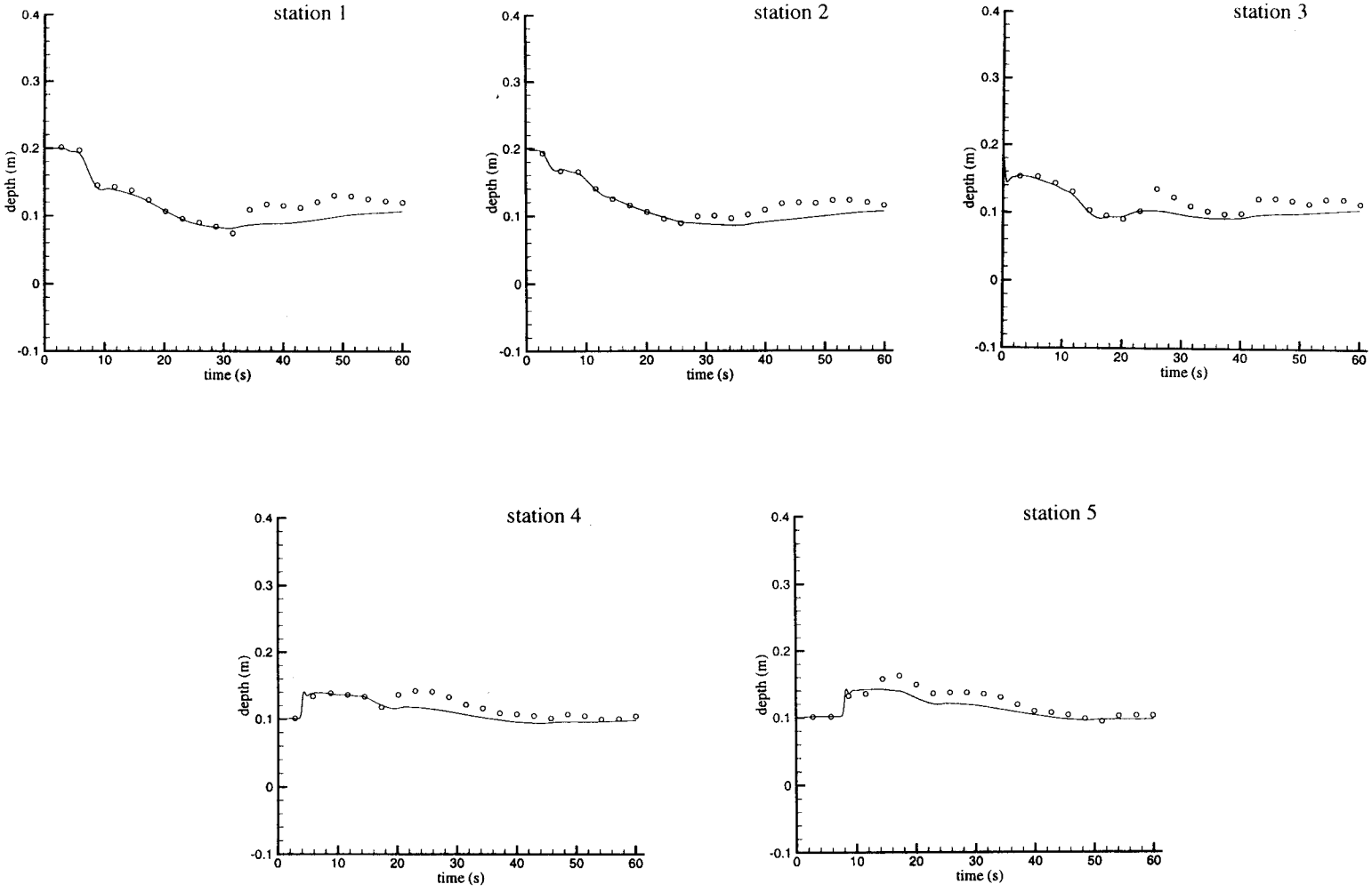

Figure 18. Comparison of numerical (—), Hicks *et al.* [17] (△) and experimental [18] (○) results for a wet bed horizontal channel.

6. CONCLUSIONS

Methods based on the FCT formulation manifest many properties desirable in numerical simulations. The conservation property, the avoidance of numerical oscillations, and the achievement of higher-order accuracy makes the FCT schemes a robust tool in capturing shocks in open channel flows. The basic flow equations that govern one-dimensional open channel flows have been solved using a FCT technique coupled with traditional finite difference techniques. After a brief description of the governing equations and development of the numerical procedure, the method's performance was tested on various open channel flow problems, including the hydraulic jump and dam break flows, both on wet and dry beds. In all cases the results were good when compared with experimental results, analytical solutions and with other published numerical results when available. The present scheme has an inherent high resolution shock capturing ability and no special (artificial) numerical smoothing is needed to dampen oscillations resulting from the shock wave. Extensive tests have been carried out to justify the robustness of the method. A test of the mass residual error at steady state shows that the present formulation is also conservative. Based on the results of this work, the authors conclude the main advantage of the FCT technique is its simplicity in coupling it to standard finite difference schemes and its robustness in handling various flow configurations.

ACKNOWLEDGMENTS

The authors would like to thank F.E. Hicks for providing their numerical data for comparison purposes.

REFERENCES

1. A. Jameson, W. Schmidt and E. Turkel, 'Numerical solutions of the Euler equations by finite volume methods using Runge–Kutta time stepping schemes', *AIAA 14th Fluid and Plasma Dynamics Conference*, Palo Alto, CA, AIAA, 1981, pp. 81–1259.
2. A. Harten, 'High-resolution schemes for hyperbolic conservation laws', *J. Comp. Phys.*, **49**, 357–393 (1983).
3. J.P. Boris and L.D. Book, 'Flux-corrected transport I: SHASTA, a fluid transport algorithm that works', *J. Comp. Phys.*, **11**, 38–69 (1973).
4. D.L. Book, J.P. Boris and K. Hain, 'Flux-corrected transport II: Generalizations of the method', *J. Comp. Phys.*, **18**, 248–278 (1975).
5. S.T. Zalesak, 'Fully multidimensional flux-corrected transport algorithms for fluids', *J. Comp. Phys.*, **31**, 335–362 (1979).
6. P. Collela and P.R. Woodward, 'The piecewise parabolic method (PPM) for gas dynamics simulation', *J. Comp. Phys.*, **54**, 174–201 (1984).
7. A. Harten and S. Osher, 'Uniformly high-order-accurate non-oscillatory schemes', *SIAM*, **24**, 279–310 (1987).
8. C.W. Shu and S. Osher, 'Efficient implementation of essentially non-oscillatory shock capturing schemes', *J. Comp. Phys.*, **77**, 439–471 (1988).
9. S.A. Yost and P. Rao, 'A non-oscillatory scheme for open channel flows', *Adv. Water Res.*, **22**, 133–143 (1998).
10. M.H. Chaudhry, *Open Channel Flow*, Prentice Hall, New York, 1993.
11. M.B. Abbott, *Computational Hydraulics: Elements of Theory of Free Surface Flows*, Pitaman, London, 1979.
12. R. Garcia and R.A. Kahawita, 'Numerical simulation of St. Venant's equations with the MacCormack finite difference scheme', *Int. J. Numer. Methods In Fluids*, **6**, 259–274 (1986).
13. A.M. Gharangik and M.H. Chaudhry, 'Numerical simulation of hydraulic jump', *J. Hydraul. Eng.*, **117**, 1195–1211 (1991).
14. M. Rahman and M.H. Chaudhry, 'Simulation of hydraulic jump with grid adaptation', *J. Hydraul. Res.*, **33**, 555–569 (1995).
15. D.A. Anderson and M.M. Rai, 'The use of solution adaptive grids in solving partial differential equations', *Proc. Symp. on Numerical Generation of Curvilinear Co-ordinates System and their use in the Numerical Simulation of Partial Differential Equations*, Nashville, TN, April 13–16, 1982.
16. D.C. Dammuller, S.M. Bhallamudi and M.H. Chaudhry, 'Modeling of unsteady flow in curved channel', *J. Hydraul. Eng.*, **115**, 1479–1495 (1988).

17. F.E. Hicks, P.M. Steffler and N. Yasmin, 'One-dimensional dam break solutions for variable width channels', *J. Hydraul. Eng.*, **123**, 464–468 (1997).
18. C.V. Bellos, J.V. Soulis and J.G. Sakkas, 'Experimental investigation of two-dimensional dam break flows', *Int. J. Hyd. Res., Delft*, **461**, 47–63 (1992).
19. T. Molls and M.H. Chaudhry, 'Depth-averaged open channel flow model', *J. Hydraul. Eng.*, **121**, 453–465 (1995).
20. R.J. Fennema and M.H. Chaudhry, 'Simulation of 1D dam break flows', *J. Hyd. Res*, **25**, 4151 (1987).
21. C.V. Bellos and J.G. Sakkas, '1D dam break flood wave propagation on dry bed', *J. Hydraul. Eng.*, **113**, 1510–1524 (1987).

